Optical phantoms for ultrasound-modulated optical tomography

Chulhong Kim, Alejandro Garcia-Uribe, Sri-Rajasekhar Kothapalli, Lihong V. Wang

Chulhong Kim, Alejandro Garcia-Uribe, Sri-Rajasekhar Kothapalli, Lihong V. Wang, "Optical phantoms for ultrasound-modulated optical tomography," Proc. SPIE 6870, Design and Performance Validation of Phantoms Used in Conjunction with Optical Measurements of Tissue, 68700M (21 February 2008); doi: 10.1117/12.766773

SPIE.

Event: SPIE BiOS, 2008, San Jose, California, United States

Optical phantoms for ultrasound-modulated optical tomography

Chulhong Kim[1], Alejandro Garcia-Uribe[2], Sri-Rajasekhar Kothapalli[1] and Lihong V. Wang[1*]

[1]Optical Imaging Laboratory, Department of Biomedical Engineering, Washington University in St. Louis, Campus Box 1097, One Brookings Dr. St. Louis, Missouri, 63130

[2]Department of Electrical Engineering, 3120 TAMU, Texas A&M University, College Station, Texas, 77843-3120

ABSTRACT

Optical phantoms are widely used for simulating optical properties of biological tissues. Their accurate design and fabrication are important factors in validating and designing biomedical systems. We discuss fabrication and measurement of optical phantoms in ultrasound-modulated optical tomography. The optical properties of the phantoms are measured by an oblique-incidence diffuse reflectance spectrometer, which can accurately measure the wavelength-dependent absorption and reduced scattering coefficients of optical phantoms. In addition, the acoustic properties of the phantoms are discussed.

Keywords: Optical phantoms, ultrasound-modulated optical tomography, oblique-incidence diffuse reflectance spectrometer, optical absorption coefficient, optical reduced scattering coefficient.

INTRODUCTION

1. Motivation

In the biomedical optics field, the use of tissue simulating phantoms has become increasingly important. The main purposes of dynamic tissue phantom include: 1. validation, design, optimization of optical systems, 2. calibration and stability test, and 3. comparison of performance between multiple systems.[1] Because of the importance of the accurate fabrication of optical phantoms, a number of tissue-phantom-modalities have been explored including solid non-organic polymers, silicone phantoms, and bio-compatible phantoms with hydrogels.[1] In addition, many optical spectroscopes are developed and utilized to accurately calibrate the optical properties of the tissue phantoms.

In this Proceedings article, by using an oblique-incidence diffuse reflectance spectrometer which can precisely calibrate the wavelength dependent absorption and reduced scattering coefficients of the tissue phantoms, we estimated the optical absorption and reduced scattering spectra of hydrogel-based phantoms mixed with intralipid or cornstarch, which are widely used as representative tissue phantoms for ultrasound-modulated optical tomography (UOT). Since the spatial resolution of UOT depends on the ultrasound parameters, the acoustic properties of the tissue phantoms are considered as well. In addition, two optically absorptive targets embedded in gelatin-intralipid based medium are successfully imaged using a ring shaped light illumination UOT system using the intense acoustic bursts and a CCD camera based speckle contrast detection technique. The image is also compared to a single element ultrasound pulse-echo image.

2. The principle of ultrasound-modulated optical tomography (UOT)

UOT[2,3] is a novel bio-photonic imaging technique which is capable of providing strong optical contrast and high ultrasonic spatial resolution. When a coherent laser illuminates an optically turbid medium under ultrasound insonification, multiple-scattered light traveling through the ultrasonic focal volume is acoustically tagged from time-varying particle displacements and changes in refractive index. By measuring the ultrasound-modulated light at each

* Corresponding author: lhwang@biomed.wustl.edu

Design and Performance Validation of Phantoms Used in Conjunction with Optical Measurements of Tissue, edited by Robert J. Nordstrom, Proc. of SPIE Vol. 6870, 68700M, (2008) · 1605-7422/08/$18 · doi: 10.1117/12.766773

scanned ultrasonic focal volume position, images map the distribution of optical properties in the medium. Theoretically, the mechanisms of UOT have been studied by Leutz *et al.*[4], Wang[5,] and Sakadžic´ and Wang[6]. Because of the low signal-to-noise ratio (SNR) in UOT, a number of detection techniques have been developed to detect weak modulated signals effectively such as parallel detection with CCD cameras[7–9], Fabry-Perot interferometer based detection[10], and photo-refractive crystal based detection[11]. Instead of exploring new detection techniques to improve SNR, Kim *et al.*[12] applied intense acoustic bursts to enhance UOT signals.

3. The principle of an oblique-incidence diffuse reflectance spectrometer (OIR)

Normal-incidence reflectometry can separate the two effects of scattering and absorption but only with absolute measurements of the multiple-scattered reflected light (diffuse reflectance). Oblique-incidence light illumination breaks the symmetry in the diffuse reflectance pattern (Figure. 1).

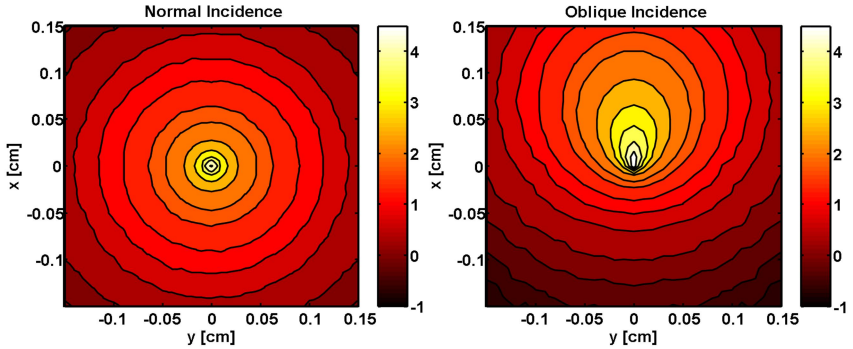

Figure 1: Normal vs. oblique incidence diffuse reflectance pattern.

The spatially resolved steady-state diffuse reflectance for particular wavelength and oblique incidence can be calculated by [13,14].

$$R(x) = \frac{1}{4\pi}\left[\frac{\Delta z(1+\mu_{eff}\rho_1)\exp(-\mu_{eff}\rho_1)}{\rho_1^3} + \frac{(\Delta z + 2z_b)(1+\mu_{eff}\rho_2)\exp(-\mu_{eff}\rho_2)}{\rho_2^3}\right] \quad (1)$$

where the effective attenuation coefficient $\mu_{eff} = (\mu_a / D)^{1/2}$, ρ_1 and ρ_2 are the distances between the source point and the observation point on the surface, Δz is the distance between the virtual boundary and the tissue depth, and z_b is the distance between the virtual boundary and the surface of the sample. The distance from the point of incidence to the positive point source $d_s = 3D$. For oblique incidence, the diffusion coefficient is

$$D = \frac{1}{3(0.35\mu_a + \mu_s')} \quad (2)$$

The parameters μ_a is the absorption coefficient and μ_s' is the reduced scattering coefficient. The shift of the point sources in the x direction, Δx (Figure 2), is

$$\Delta x = \frac{\sin(\alpha_t)}{0.35\mu_a + \mu_s'} \quad (3)$$

where α_t is the angle of light transmission into the tissue. Using simple geometrical transformations the absorption and reduced scattering coefficients can be calculated by

$$\mu_a = \frac{\mu_{eff}^2 \Delta x}{3\sin(\alpha_t)} \quad (4)$$

$$\mu_s' = \frac{\sin(\alpha_t)}{\Delta x} - 0.35\mu_a \quad (5)$$

The diffusion equation assumes that the reduced scattering coefficient is much larger than the absorption. The source and detector must also be separated in space so that the light is diffused when it reaches the detector. The Fig. 2 shows the diffused reflectance far from the source for a particular wavelength.

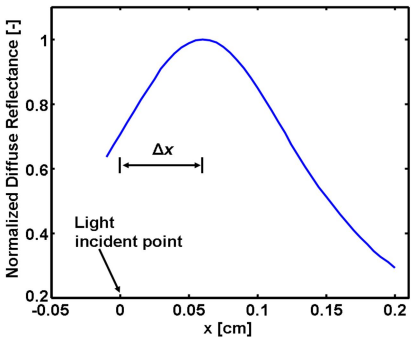

Figure 2: Schematic representation of obliquely incident spatially resolved diffuse reflected light.

EXPERIMENT

4. Phantom recipe

In UOT, hydrogels such as agar and gelatin are widely used as phantom matrix materials since they can form relatively stiff and biocompatible matrices which limit the water mobility and allow inclusion of optical targets with any shape.[1] Intralipid solution or cornstarch is used as scattering agent in UOT. To mimic the different kinds of optically absorptive objects, many types of dyes are added to the hydrogel-scattering agent mixture independently: Trypan blue dye for deoxygenated blood, Fiesta Red ink (PenCity, Georgia) for oxygenated blood and Black India ink for general absorptive objects. The fabrication procedure of hydrogel-based phantoms is as follows;

1) Add 10g of gelatin or 2g of agar to 100ml cold water.
2) Heat the mixture on the heater with a magnetic stirrer until the liquid turns to be transparent.
3) Add the different concentrations of intralipid solution or cornstarch to form various optical scattering coefficients.
4) Pour the hydrogel-scattering agent mixture into any shape of mold and wait until it becomes solid.
5) For absorptive objects, add dyes with preferable concentrations to the hydrogel-scattering agent compounds and congeal it.

Figure 3 shows the typical shape of gel-intralipid phantom (97 x 97 x 20 mm along the *X*, *Y*, and *Z* axes). One absorptive target is embedded in the middle of the slab along the *Z* axis in Figure 2C.

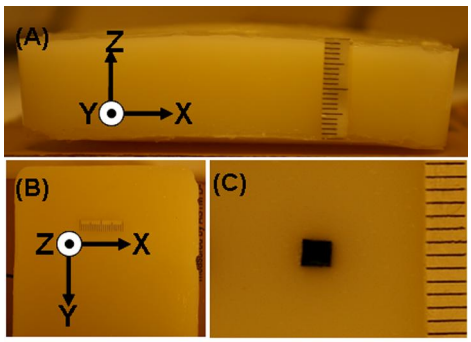

Figure 3: The photographs of a typical gel-intralipid phantom; (A) the side view, (B) the top view, and (C) an absorptive target buried in the center of the phantom.

5. Experimental setup of oblique-incidence diffuse reflectance spectroscopy system

The schematic of the system is illustrated in Figure 4. White light from a halogen lamp is coupled to an optical fiber (200 μm diameter). The fiber optic probe consists of five source fibers and 24 collection fibers. The outer source fibers are situated at 45 degrees and the remaining source fibers were placed at 25 degrees. An optical multiplexer permits light delivery delivering light through only one source fiber at a time to the area of interest. Once the light is delivered to the phantom, it interacts with the medium and the diffuse reflectance is collected by another set of optical

fibers (100 μm diameter). The collection fibers are coupled with an imaging spectrograph that generates an optical spectrum for each fiber. A CCD camera collects the spectral-images for the selected wavelength range.

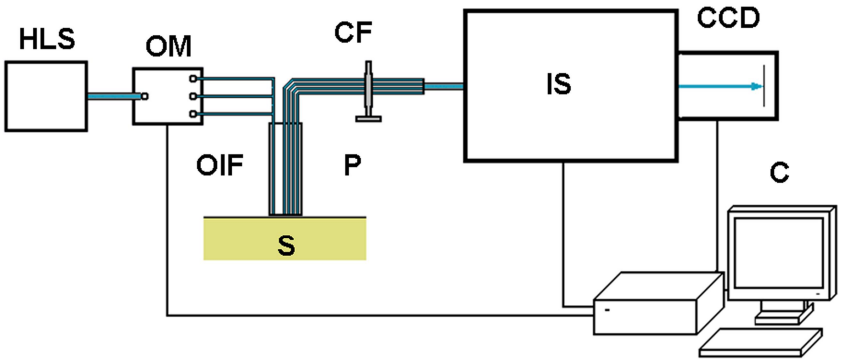

Figure 4: The OIR experimental setup: HLS, halogen light source; CCD, CCD camera; OM, optical multiplexer; OIF, oblique incidence fibers; CF, collection fibers; P, probe; S, sample; IS, imaging spectrograph; C, computer.

6. Experimental setup of ultrasound-modulated optical tomography

The experimental setup of the UOT system is schematically drawn in Fig. 5. The donut-shaped light illumination is formed by a plano-concave lens, a spherical conical lens, and an optical condenser in respective order. A diode laser (Melles Griot, 56ICS153/HS; 657-nm wavelength, 9 × 6 × 13 cm along the *X*, *Y*, and *Z* axes) mounted on the same post as optics illuminates tissue phantoms with an average power of ~24.5 mW/cm^2. A 7.5MHz focused ultrasound transducer (Panametrics, A320S-SU; 12.7 mm active aperture; 19.7 mm focal length) placed into the middle of the optical condenser generates acoustic waves. The transducer surface is immersed in water inside a water tank. The bottom of water tank is sealed with a thin disposable clear membrane. In addition, the line focus of light is aligned with the ultrasonic focus in water. The peak pressure of 3.6MPa is applied to the ultrasonic focal point, so the mechanical index at this frequency is 1.3, which is within the typical safety limit for diagnostic ultrasound.[15] The sample holder inside the water tank is connected to an automatic scanning stage for raster scanning. A CCD camera (Basler, A312f; 12-bit, 640×480 pixels) located underneath the water tank captures speckle patterns yielded from the sample. 1 ms acoustic bursts are synthesized by a function generator (Agilent, 33250A) and subsequently amplified by an RF amplifier (ENI, Inc., 325LA) to drive the ultrasound transducer. A pulse-delay generator (Stanford Research, DG535) triggered by the burst initiation produces two CCD trigger pulses for each burst. One burst-synchronized frame is captured on the CCD camera with ultrasound effect, and the other is taken without any ultrasound effect. A low 0.83-Hz duty cycle is used to prevent damage to the transducer. We measure laser speckle contrast on the CCD surface with and without the ultrasound modulation. Therefore, we define our signal as the difference between ultrasound ON and OFF in speckle contrast measurements and average 2 pairs of on-off measurements.

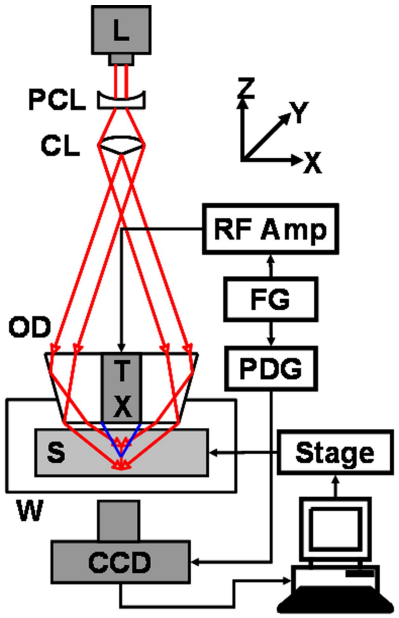

Figure 5: The UOT experimental Setup: L, laser; CCD, CCD camera; RF amp, RF amplifier; FG, function generator; PDG, pulse-delay generator; TX, ultrasound transducer; S, sample; Stage, mechanical scanning stage; W, water tank; PCL, plano-concave lens; CL, conical lens; OD, optical condenser.

RESULTS AND DISCUSSIONS

1. Optical spectra of tissue mimicking phantoms

The oblique incidence diffuse reflectance spectroscopy system can be used to design an optical phantom with desired optical properties. First a phantom made of 2g of agar, 4.5ml of 20% intralipid, 5mg of Trypan blue dye, and 100ml of water is measured. Figure 6 shows the absorption coefficient (Fig. 6A) and reduced scattering coefficient (Fig. 6B) spectra. The experimental results are compared to the optical properties of soft tissues[16] such as skin (dermis), arm, forehead, and breast in Fig. 6. In addition, the amount of intralipd or Trypan blue dye can be increased or reduced in order to match the desired reduced scattering or absorption coefficients. To investigate the variation of the reduced scattering coefficient according to the concentration of scattering particles, we measured a phantom made of 10g of gelatin and 100ml of water with varying the concentration of cornstarch from 20g to 40g. As the concentration of cornstarch mounts, the reduced scattering coefficient is increased linearly in Fig. 7.

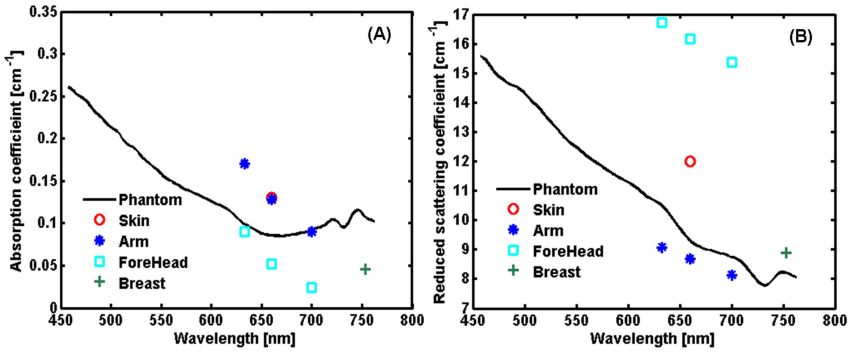

Figure 6: Optical spectra of an agar-intralipid based phantom: (a) the absorption coefficient and (b) the reduced scattering coefficient.

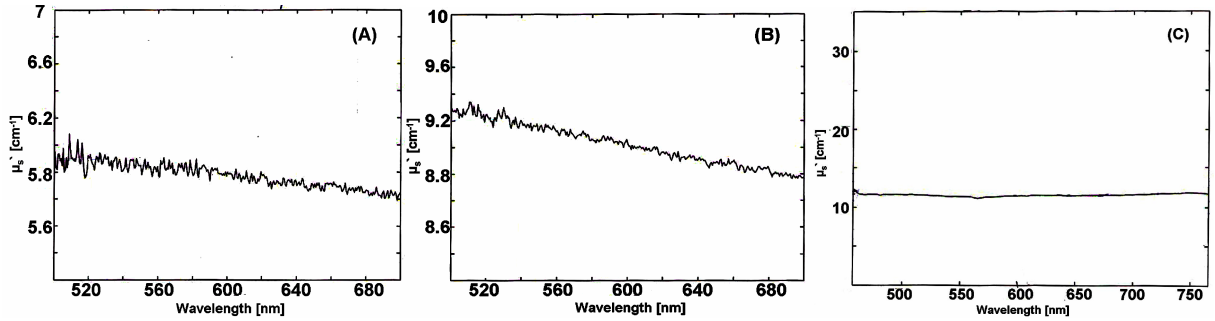

Figure 7: The reduced scattering coefficient spectra of gelatin-cornstarch based phantoms with varying the concentration of cornstarch: (a) 20 g, (b) 30 g, and (c) 40 g of cornstarch with 10g of gelatin and 100ml of water.

2. Acoustic properties of tissue mimicking phantoms

Since the light modulation is created by the ultrasound-light interaction, the acoustic properties of tissues also need to be considered in UOT. If the mechanical property of the inside target is different from the one of the background medium, UOT can provide the mechanical property difference of two materials. Recently, Xu *et al*.[17] and Bossy *et al*.[18] reported the measurement of mechanical properties of tissues using UOT in detail. In this study, however, our study is only based on the heterogeneities of optical properties in tissue phantoms. Therefore, in this section, we studied mechanical bio-compatibilities of our hydro-gel based phantoms to soft biological tissues. The table 1[19-25] shows the brief comparisons of acoustic properties such as frequency dependent attenuation, speed of sound, and Young's modulus between the hydro-gel based phantoms and various soft tissues. The acoustic properties of hydro-gel phantoms are close to the properties of soft tissues like breast fat, liver, and muscle in Table 1.

Materials	Frequency dependent attenuation (dB cm^{-1} MHz^{-1})	Speed of sound (m/s)	Young's modulus (Pa)
Hydrogel-phantom	0.5	1540	16K
Breast fat	0.55	1430	1K
Liver	0.5	1580	5K
Muscle	1.1	1580	
Blood	0.18	1570	
Lung	41	700	
Bone	20	3500	5G

Table 1: Acoustic properties of hydro-gel phantoms and various biological tissues.

3. 2D images

To investigate the validation of the tissue phantoms for UOT, we imaged a gelatin-intralipid phantom (10% gelatin by weight and 1% intralipid by volume) containing two optically absorptive targets (2 mm × 2 mm × 2 mm) separated by 10 mm from center-to-center. The total thickness of the slab was about 2 cm and two objects were buried in the middle. The mechanical properties of two objects were identical to the surrounding phantom. Two absorbing objects are clearly seen in Fig. 8B and match well with the ones in Fig. 8A photograph, whereas the light intensity based image in Fig.8C cannot resolve two objects. Moreover, two objects are not clearly resolvable in the pulse-echo imaging, Fig.8D since the mechanical properties of the objects are identical to the background medium.

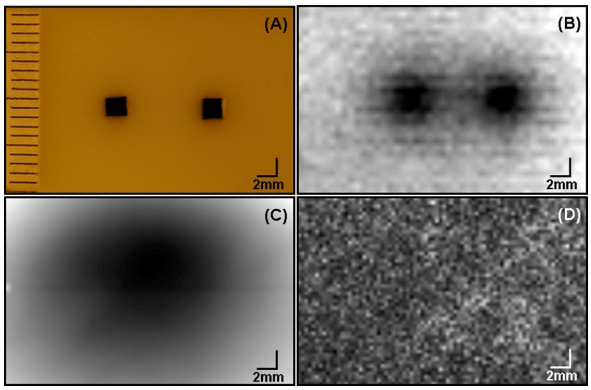

Figure 8: 2D images of the two absorptive targets. (A) A photograph of two targets. (B) UOT image. (C) Light intensity based image. (D) Single-element ultrasound pulse-echo image.

CONCLUSIONS

In summary, we studied the optical and acoustic properties of tissue simulating phantoms used in ultrasound-modulated optical tomography. The measured optical properties, the absorption and reduced scattering coefficients, of hydro-gel based phantoms using the oblique-incidence diffuse reflectance spectrometer were compared to the literature data. Since the mechanisms of UOT are based on the light-ultrasound interaction, the acoustic properties of the tissue phantoms were studied and compared to the ones of biological tissues. Optically absorptive targets compared to the background medium were successfully imaged using the UOT system, while the pulse-echo imaging could not provide the difference between targets.

ACKNOWLEDGEMENT

This research was supported by the National Institutes of Health grants CA094267 and CA106728.

REFERENCES

[1] B. W. Pogue, M. S. Patterson, “Review of tissue simulating phantoms for optical spectroscopy, imaging and dosimetry,” J. Biomed. Opt. 11, pp. 041102.1-041102.16 (2006).
[2] F. A. Marks, H. W. Tomlinson, and G. W. Brooksby, “Comprehensive approach to breast cancer detection using light: photon localization by ultrasonic modulation and tissue characterization by spectral discrimination,” in Photon Migration and Imaging in Random Media and Tissue, B. Chance and R. R. Alfano, eds., Proc. SPIE 1888, pp. 500–510 (1993).
[3] L.-H. Wang, S. L. Jacques, and X. Zhao, “Continuous-wave ultrasonic modulation of scattered laser light to image objects in turbid media,” Opt. Lett. 20, pp. 629–631 (1995).
[4] W. Leutz, G. Maret, “Ultrasonic modulation of multiply scattered light,” Phys. B 204, pp. 14–19 (1995).
[5] L.-H. V. Wang, “Mechanisms of ultrasonic modulation of multiply scattered coherent light: an analytic model,” Phys. Rev. Lett. 87, (043093) pp. 1–4 (2001).
[6] S. Sakadžic´, L.-H. Wang, "Correlation transfer and diffusion of ultrasound-modulated multiply scattered light," Phys. Rev. Lett. 96, 163902 pp. 1–4 (2006)
[7] S. Leveque, A. C. Boccara, M. Lebec, and H. Saint-Jalmes, “Ultrasonic tagging of photon paths in scattering media: parallel speckle modulation processing,” Opt. Lett. 24, pp. 181–183 (1999).
[8] G. Yao, S. Jiao, and L.-H. Wang, “Frequency-swept ultrasound-modulated optical tomography in biological tissue by use of parallel detection,” Opt. Lett. 25, pp. 734–736 (2000).
[9] M. Gross, P. Goy and M. Al-Koussa, “Shot-noise detection of ultrasound-tagged photons in ultrasound-modulated optical imaging,” Opt. Lett. 28, pp. 2482-2484 (2003).
[10] S. Sakadžic´, L.-H. V. Wang, “High-resolution ultrasound-modulated optical tomography in biological tissues,” Opt. Lett. 29, pp. 2770-2772 (2004).

[11] T. W. Murray, L. Sui, G. Maguluri, R. A. Roy, A. Nieva, F. Blonigen, C. A. DiMarzio, "Detection of ultrasound-modulated photons in diffuse media using the photorefractive effect," Opt. Lett. 29, pp. 2509-2511 (2004).
[12] C. Kim, R. J. Zemp, and L. V. Wang, "Intense acoustic bursts as a signal-enhancement mechanism in ultrasound-modulated optical tomography," Opt. Lett. 31, pp. 2423–2425 (2006).
[13] L. -H. Wang, S. L. Jacques, "Use of a laser beam with an oblique angle of incidence to measure the reduced scattering coefficient of a turbid medium," Appl. Opt. vol. 34,, pp. 2362-2366, (1995).
[14] S. -P. Lin, L. Wang, S. L. Jacques, and F. K. Tittel, "Measurement of tissue optical properties by the use of oblique-incidence optical fiber reflectometry," Appl. Opt. vol. 36, no. 1, pp. 136-143, (1997).
[15] Diane Dalecki, "Mechanical bioeffects of ultrasound," Annu. Rev. Biomed. Eng. **6**, pp. 18.1–18.20 (2004).
[16] Valery Tuchin, "Tissue Optics: Light scattering Methods and Instruments for Medical Diagnosis," The Society of Photo-Optical Instrumentation Engineers, (2000).
[17] X. Xu, H. Zhang, D. Qing, C. Kim, P. Hemmer, L. V. Wang, "Photorefractive detection of tissue optical and mechanical properties by ultrasound modulated optical tomography," Opt. Lett. 32, pp. 656–658 (2007).
[18] E. Bossy, A. R. Funke, K. Daoudi, and A. Boccara, "Transient optoelastography in optically diffusive media," Appl. Phys. Lett. 90, pp. 174111.1–174111.3 (2007).
[19] J. L. Prince and J. M. Links, "Medical Imaging Signals and Sytems," Pearson Prentice Hall, (2006).
[20] C. R. Hill, J. C. Bamber, and G. R. ter Harr, "Physical Principles of Medical Ultrasonics, 2nd Edition," Wiley, (2004).
[21] E. Turgay, S. Salcudean, and R. Rohling, "Identifying the mechanical properties of tissue by ultrasound strain imaging," Ultrasound in Med. & Biol., 32, pp. 221–235 (2006).
[22] N. Kudo, M. Yoshida, K. Yamamoto, T. Mikami, A. Kitabatake, and Y. Ito, "Basic study on the ultrasound attenuation of fibrous biological tissue in the frequency range of 10-40 MHz," IEEE Ultrasonics Symposium,. pp. 1479–1482, (1998).
[23] F. R. Pereira, J. C. Machado and W. C. A. Pereira, "Ultrasonic wave speed measurement using the time-delay profile of rf-backscattered signals: Simulation and experimental results," J. Acoust. Soc. Am. 111, pp. 1445–1453 (2002).
[24] J. E. Browne, K. V. Ramnarine, A. J. Watson and P. R. Hoskins, "Assessment of the acoustic properties of common tissue mimicking test phantoms," Ultrasound in Med. & Biol. 29, pp. 1053–1060 (2003).
[25] W. D. D'Souza, E. L. Madsen, O. Unal, K. K. Vigen, G. R. Frank, and B. R. Thomadsen, "Tissue mimicking materials for a multi-imaging modality prostate phantom," Med. Phys. 28, pp. 688–700 (2001).